JOURNAL OF PROPULSION AND POWER
Vol. 17, No. 5, September–October 2001

Underexpanded Jet for Testing Laser-Based Combustion Diagnostics

K. G. Klavuhn* and J. C. McDaniel†
University of Virginia, Charlottesville, Virginia 22903

The design, construction, and operation of an underexpanded jet facility developed as a test flowfield for laser-based supersonic combustion diagnostics are described. The continuous-running device accelerates hot gases from a 160-kPa, 2000-K, stoichiometric H_2/Air combustion chamber through a 3.15-mm i.d. alumina tube into a 11-kPa chamber. The resulting underexpanded jet of flame species provides a range of flowfield parameters (M = 1–4, T = 1700–500 K, P = 72.8–2.7 kPa, and ρ = 0.12–0.004 kg/m^3) typical of practical supersonic combustion experiments. The modeling of the jet flowfield using an axisymmetric Navier–Stokes code is also described.

Introduction

UNDEREXPANDED jets are particularly attractive as test flowfields for high-speed compressible flow diagnostics because they are reproducible, have been studied extensively,[1–15] can be modeled with good accuracy,[16–22] and offer a broad range of the important measurable parameters. For these reasons extensive use has been made of jets in the development of laser-based diagnostic techniques for use in high-speed, nonreacting compressible flows. Nonintrusive techniques for the measurement of density,[23,24] velocity,[24–26] pressure,[26] and temperature[27] using laser-induced fluorescence (LIF) of I_2 seeded in air have been studied using underexpanded jets. Other techniques for velocity measurement in nonreacting flows using LIF of NO seeded in air,[28,29] LIF of Na seeded in nitrogen,[30] LIF probing of vibrationally tagged O_2 in unseeded air,[31,32] LIF probing of OH produced by the photodissociation of water vapor in air,[33] inverse Raman spectroscopy of N_2,[34] Raman gain spectroscopy of N_2,[35] and coherent anti-Stokes Raman spectroscopy of CH_4,[36] have been also been studied using supersonic jets.

Renewed interest in propulsion systems for hypersonic aircraft and reusable launch vehicles using combined airbreathing/rocket cycles has created a need for nonintrusive diagnostic techniques that are effective in high-speed combusting flows. Calibration of these new techniques requires a flowfield with gasdynamic and thermodynamic conditions similar to those found in the model supersonic combustors in which the techniques are to be applied. Brief descriptions of jet facilities incorporating flame products have appeared in the literature. For example, a supersonic, axisymmetric freejet was formed by exhausting the products from a high-pressure (~405 kPa), stoichiometric CH_4/Air flame through a 1.6-mm diam nozzle into ambient air and used for the demonstration of a technique for measuring velocity, temperature, and pressure using rapid continuous-wave wavelength-modulation LIF of OH.[37] A similar high-pressure (~172 kPa) H_2/Air diffusion flame combustor with a 3.2-mm diam nozzle was used to produce a subsonic jet for demonstrating velocity and temperature measurements using XeCl excimer LIF of OH.[38] In another experiment a supersonic freejet produced by expanding the combustion products of a low-pressure (7 kPa) H_2/O_2/Ar flame through a 4.56-mm diam nozzle was used for the demonstration of rotational temperature measurements using LIF of OH.[39] However, the design, construction, operation, and characterization of these facilities are not discussed in detail.

In this article, a unique underexpanded jet facility that was constructed for the testing of supersonic combustion diagnostics intended for use in model supersonic combustion ramjet combustors is described. The facility is small and inexpensive and produces a well-controlled, high-speed, low-pressure flowfield of combustion species without the use of vacuum pumps. The design, operation, and characterization of the jet are presented, including an analysis of the distribution of flow properties in the jet's supersonic core.

Design Features

A cross section of the underexpanded jet facility is shown in Fig. 1, and a schematic of the entire setup is shown in Fig. 2. The fuel and air enter a small mixing chamber on top of the facility. The fuel stream is oriented between two counterpropagating airstreams in order to promote mixing. The fuel/air mixture passes into the combustion chamber through a multiholed orifice plate located at the bottom of the mixing chamber. The size of the burner holes was determined by estimating the total mass flow rate and sizing the holes so that the flow speed through each hole would be at least twice the maximum projected laminar flame speed.[40] This ensures that the flame cannot flash back into the mixing chamber, while not restricting adjustability of the flow rates when using constant pressure supplies by creating a sonic throat in the flowpath. In addition, in-line filters with 7-μm sintered elements were installed in the fuel and air lines at the inlets of the mixing chamber to snub the flame in the event of flashback and to prevent pressure fluctuations from resonating in the supply lines causing flow instabilities. The fuel and airflow rates are controlled with course and fine metering valves mounted in parallel and monitored using mass flowmeters for precise adjustment of the total flow rate and equivalence ratio.

A spark generator produces a spark between a nichrome ignitor and the burner surface to initiate combustion. The ignitor enters the combustion chamber through one of four access ports located symmetrically around the burner. The flame burns below the burner surface and is contained in an insulated combustion chamber. A machinable ceramic was used to form the insulation to protect the aluminum shell of the combustion chamber from the hot flame gases and to reduce the quenching of flame radicals at the inside wall by allowing the surface to remain hot. The pressure of the combustion chamber is monitored by a pressure transducer, which accesses the chamber through one of the remaining three access ports. The two remaining ports can be used for monitoring the chamber temperature and/or for adding seed species, such as NO or Na, or seed particles for LDV and other Mie scattering techniques, to the flow.

Once ignited, the reacting mixture is accelerated through a 38.1-mm-long, 3.15-mm i.d. alumina tube into a low-pressure chamber to form an axisymmetric, underexpanded, supersonic freejet. The alumina tube provides a rugged, high-temperature boundary

Received 7 December 2000; revision received 7 May 2001; accepted for publication 30 May 2001.

*Graduate Research Assistant, Aerospace Research Laboratory, Department of Mechanical and Aerospace Engineering; currently Staff Development Engineer, Lumenis Inc., 1249 Quarry Lane, Suite 100, Pleasanton, CA 94566. Student Member AIAA.

†Professor, Aerospace Research Laboratory, Department of Mechanical and Aerospace Engineering. Member AIAA.

that minimizes quenching of the flame radicals while improving the structural integrity of the thin-walled ceramic nozzle exit. An alumina cement was used to bond the alumina tube to the surrounding insulation and to repair occasional cracks in the insulation caused by thermal stress. The low-pressure chamber is pumped by a remote set of air ejectors, which provide an adjustable backpressure that is monitored by a vacuum transducer connected to the low-pressure chamber through a port in the wall. In-line filters with 7-μm sintered elements were also installed in the lines connecting the pressure and vacuum transducers to the combustion and low-pressure chambers to prevent any high-frequency pressure fluctuations from resonating in the lines.

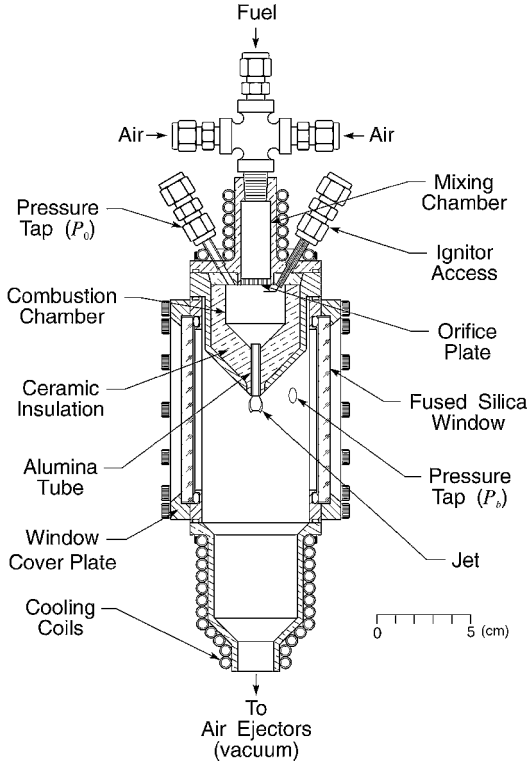

Fig. 1 Cross-section view of the underexpanded jet facility.

Three 150 × 50 × 6.4-mm-thick fused silica windows, centered on the underexpanded jet, provide generous access for laser beam transmission and signal collection. In addition, the combustion chamber wall and window cover plate edges are tapered, forming a 45-deg angle with the centerline of the alumina tube, to allow up to 45-deg access to the flowfield in the vertical plane. Aluminum blanks with mounts for smaller, less expensive windows are substituted when full optical access is not required. Water cooling is applied to the brass mixing chamber/burner and exhaust assemblies, enabling the jet to be operated continuously without overheating. The jet is oriented in a vertical sense with the flame products exhausting out the bottom to prevent condensates from contaminating the windows—a problem that is experienced with most flat flame facilities where the exhaust is above the flame.

In the present configuration all of the electronic sensors are connected to a laboratory PC via a IEEE-488 bus to allow convenient recording of the operating conditions during experiments. A flexible section in the exhaust line and three precision translation stages, mounted to the back of the low-pressure chamber, enable precise positioning of the jet in three axes. For safety, the entire jet assembly is housed in a Plexiglas® enclosure that is continually exhausted to the outside atmosphere by a high-volume air ejector. In addition, a flammable gas detector is mounted in the top of the enclosure to detect any fuel leaks, and solenoid valves were installed to enable automatic shutdown and purge (with N_2) of the fuel lines in the event of a leak. These precautions are particularly necessary when using fuels such as hydrogen.

Operational Procedure

The start-up procedure begins by turning on the air ejectors and cooling water and setting the air supply to the mixing chamber with the needle valves to the level required for the desired operating conditions. The spark is turned on, and the fuel flow rate is increased with the coarse needle valve until ignition occurs. Ignition is evident

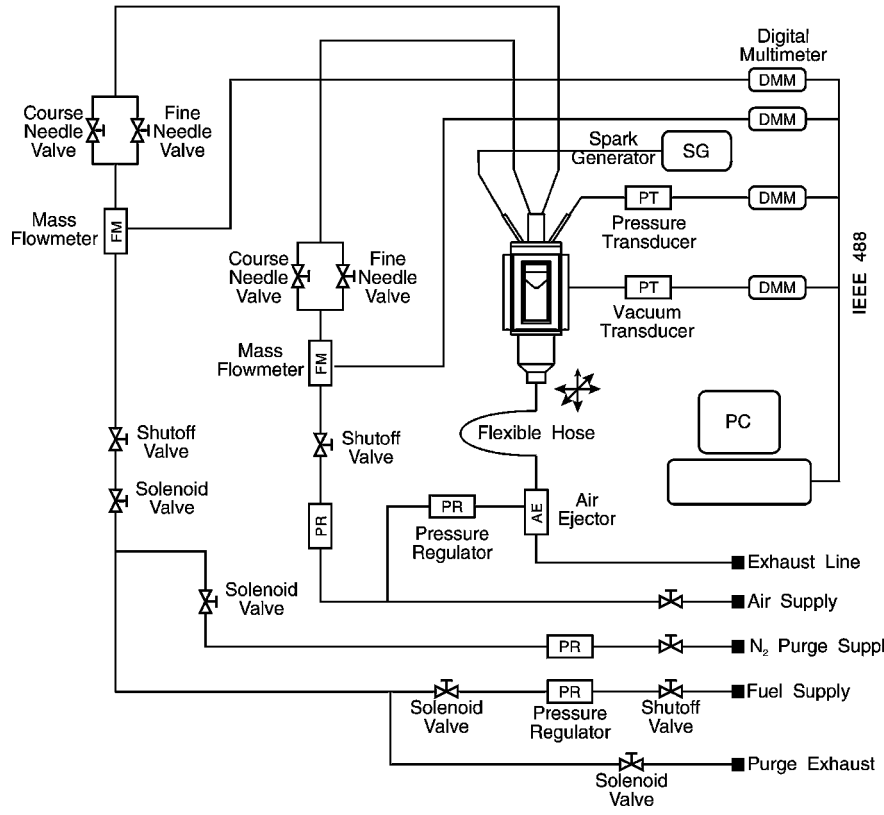

Fig. 2 Schematic of the complete underexpanded jet setup.

by the immediate increase in pressure in the combustion chamber. Once ignition is sustained, the spark is turned off, and the flow rate of the fuel is slowly (over a period of ~10 min) increased with the metering valves until the desired operating condition is reached. This procedure is recommended in order to minimize the thermal shock to the fragile ceramic insulation. Once started, the jet can run continuously, assuming that enough air, fuel, and cooling water is available.

As with the startup procedure, similar care is recommended during shutdown to avoid stressing the insulation. The fuel flow rate is slowly (over a period of ~10 min) decreased using the metering valves to the level where ignition was initially achieved, and the air and fuel are shut off simultaneously using the shut-off valves to prevent cold air from entering the combustion chamber in the absence of the flame and shocking the hot insulation. The metering valves controlling the fuel are now set for easy startup during the next experiment. A bypass valve in the vacuum line leading to the air ejectors is opened for a few minutes to allow dry air to remove any remaining condensation in the exhaust piping. The air ejectors are then shut off. The cooling water is turned off after an additional 10 min.

This facility was originally developed using propane as the fuel because it required fewer safety precautions. Although the propane flame conveniently provided enough chemiluminescence to clearly see and photograph the underexpanded jet structure that formed at the exit of the alumina tube, it was noticeably unstable and tended to deposit soot on the windows. Propane was abandoned for the desired fuel, hydrogen, once the operation of the system had been checked out. The jet was usually operated with a stoichiometric mixture of hydrogen and air. The hydrogen was supplied to the metering valves at 414 kPa and a rate of $2.34(10)^{-5}$ kg/s (15.6 SLPM) allowing 6.5 h of run time on one standard DOT-3AA2265 bottle. The air was supplied to the metering valves at 690 kPa and a rate of $8.00(10)^{-4}$ kg/s (37.2 SLPM) while the four air ejectors were supplied with 552 kPa air at a rate of $4.76(10)^{-2}$ kg/s (2209 SLPM) for a total required airflow of $4.84(10)^{-2}$ kg/s (2251 SLPM). At these flow rates the pressure in the combustion chamber was $P_0 = 160$ kPa (1.58 atm), and the backpressure was $P_b = 11$ kPa (0.11 atm).

Underexpanded Jet Flowfield

Figure 3 shows an actual photograph of the luminescent underexpanded jet plume and a schematic outlining the main features of the flowfield. The high-pressure gas leaving the exit of the tube undergoes rapid expansion into the lower pressure of the surrounding chamber. The condition of constant pressure along the jet boundary causes the expansion waves to reflect off the boundary as compression waves and also causes the boundary to be bent back toward the flow. The curvature of the jet boundary causes the compression waves to coalesce, forming the characteristic barrel shock in the interior of the jet. The barrel shock is an oblique shock, behind which the flow is still supersonic but at a lower Mach number than the flow in the core of the jet.

For slightly underexpanded jets these barrel shocks meet at the jet axis, forming the familiar diamond structure. As the pressure ratio across the nozzle is increased, the barrel shocks no longer meet at the jet axis but are connected with a normal shock or Mach disk (sometimes referred to as a Riemann wave), as pictured in Fig. 3. The Mach disk is a slightly curved shock that is normal to the flow at the jet axis. The flow immediately behind the Mach disk is clearly subsonic, whereas the flow behind the shock that reflects from the interaction of the barrel shock and the Mach disk, known as the triple point, is still supersonic. In either case the reflected barrel shocks intersect with the jet boundary reflecting as expansion waves, and the whole process is repeated until viscous effects dissipate enough of the kinetic energy of the flow that the wave structure is no longer observed.

For highly underexpanded jets, as shown in Fig. 3, only one Mach disk is present. In this case the flow behind the Mach disk acts as a potential core, which diminishes in diameter and forms a throat-like region as it adjusts to, and exchanges momentum with, the adjacent supersonic stream. The resulting reacceleration can cause the core flow to become sonic in the throat-like region.

SPARK Flowfield Calculation

The flowfield properties for a stoichiometric (i.e., equivalence ratio $\Phi = 1$) hydrogen/air jet with a source temperature $T_0 = 2000$ K, source pressure $P_0 = 160$ kPa (1.58 atm), and backpressure $P_b = 11$ kPa (0.11 atm) were calculated using an axisymmetric version of SPARK. SPARK is a Reynolds-averaged, Navier–Stokes code with finite-rate chemistry that uses a nine-species (H_2, O_2, H_2O, OH, H, O, HO_2, H_2O_2, and inert N_2), 18-reaction chemistry model.[41] SPARK uses a modified-MacCormack, finite difference technique to solve the Navier–Stokes and species continuity equations. Momentum, heat, and mass diffusion are modeled by relations based on kinetic theory. Chemistry is defined by a multicomponent finite-rate scheme, and a real-gas thermodynamics model is employed. The particular version of SPARK used here included a choice of three turbulence models: 1) laminar flow (i.e., no turbulence), 2) a mixing length model for boundary-layer applications, and 3) the algebraic model of Baldwin–Lomax for separated flows. The turbulent interaction of most interest in the underexpanded jet occurs within the free shear layers. Because the mixing length and Baldwin–Lomax models are not intended for free shear layers, the calculations were performed with the laminar option. The lack of an appropriate turbulence model was not expected to have any appreciable effect on the solution in the jet core, the region of interest in this work. Convergence was assumed when fluctuations in the density and temperature contours between iterations became less

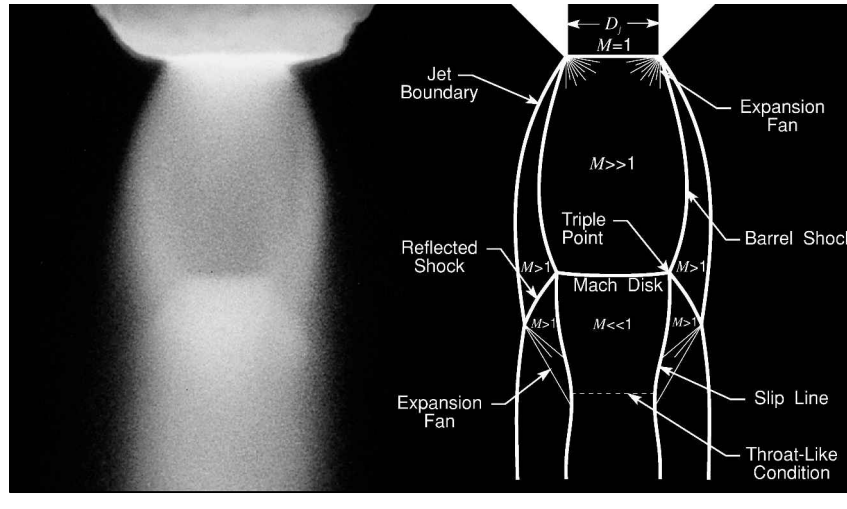

Fig. 3 Photograph of the luminescent underexpanded C_3H_8/Air jet plume (ASA 400, f/4, 25-s exposure) and schematic outlining the main features of the flowfield.

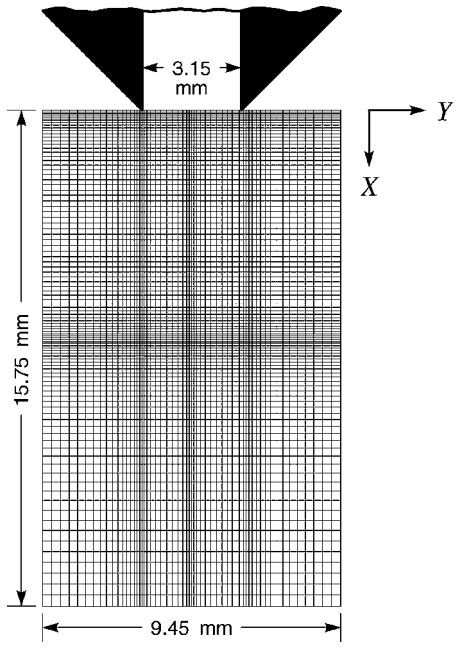

Fig. 4 Computational grid for SPARK calculation of the underexpanded jet flowfield.

than 0.1%. To smooth any residual numerical oscillations, the last 200 iterations were averaged for the final output.

Computational Grid

The 60×100 computational grid for the axisymmetric SPARK calculation of the underexpanded jet flowfield is shown in Fig. 4. Actual computations included only half of the grid shown because the flow is axisymmetric. This particular mesh size was a compromise between spatial resolution and computation time. The computational domain extended from the jet centerline to 3.0 jet radii (4.73 mm) in the transverse Y direction and from the nozzle exit to 10.0 jet radii (15.75 mm) downstream in the axial X direction. The grid was compressed in the regions of the transonic inlet, the free shear layer, and the Mach disk in order to resolve the sharp gradients expected in these areas. The expected Mach disk location was determined by first performing the calculation on a coarse uniform grid.

SPARK Boundary Conditions

Inlet

The conditions in the combustion chamber were determined using STANJAN,[42] a robust computer program that uses the element potential method for calculating the equilibrium composition of a mixture of gases. An equilibrium mixture consisting of H_2, O_2, H_2O, OH, H, O, HO_2, H_2O_2, and N_2 was calculated for the combustion chamber total conditions $T_0 = 2000$ K and $P_0 = 160$ kPa. The conditions at the exit of the ceramic tube were determined by first

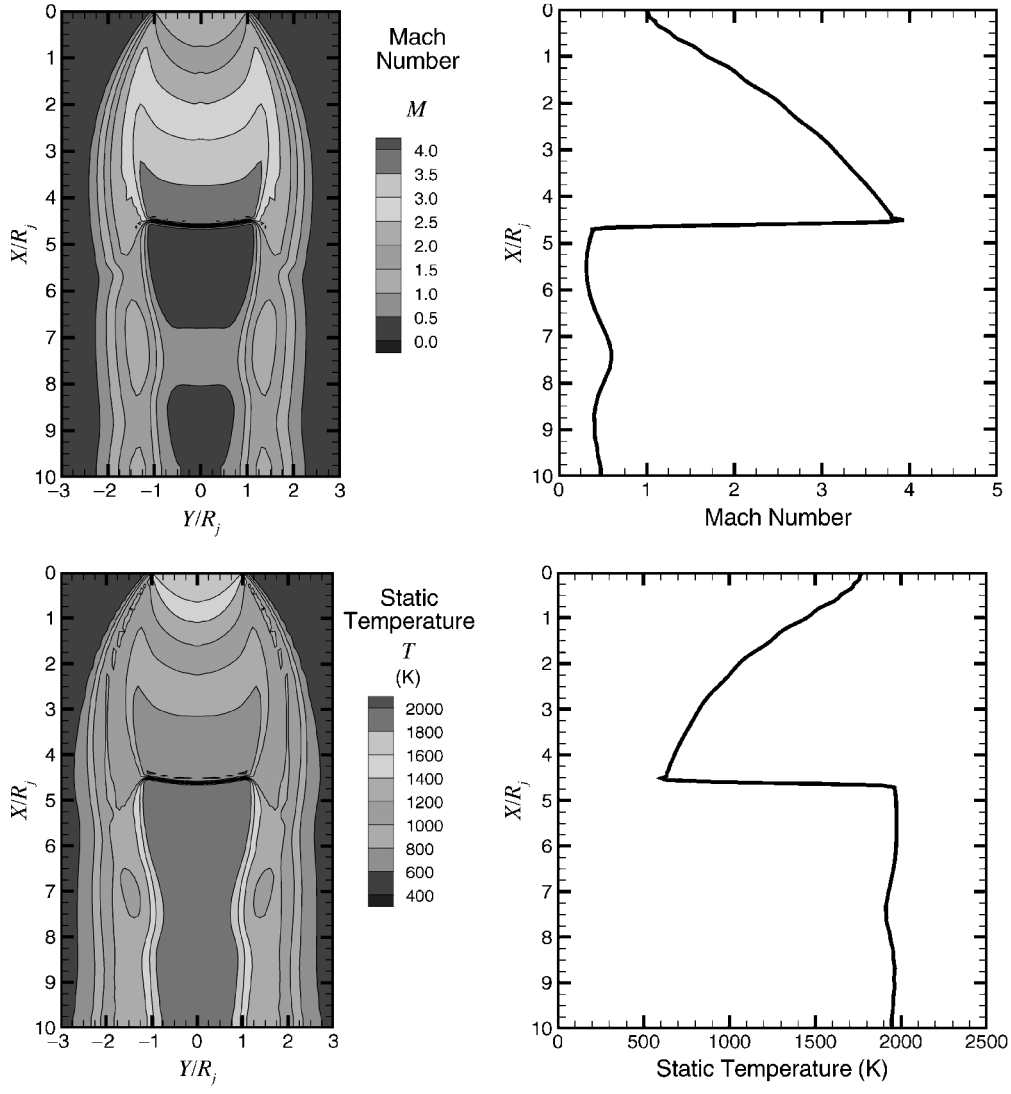

Fig. 5 Calculated contours and centerline distributions of Mach number and temperature in the underexpanded jet, where $P_0 = 160$ kPa (1.58 atm), $T_0 = 2000$ K, $P_b = 11$ kPa (0.11 atm), and $\Phi = 1.0$ (H_2/Air).

expanding the equilibrium mixture to the entrance of the alumina tube, assuming one-dimensional isentropic flow and frozen chemistry. The frozen mixture was then further expanded to $M_{ex} = 1$ at the exit of the alumina tube, assuming one-dimensional adiabatic flow with friction (Fanno line).[43] The flow in the alumina tube is not actually adiabatic. The actual heat transfer, which was not known, was accounted for by adjusting T_0 (to be discussed later). The Mach number at the entrance of the alumina tube $M_{en} = 0.58$, represents the conditions necessary at the entrance to obtain sonic flow at the tube exit. This value was determined by backcalculating from the tube exit using the Fanno-line relations. For the Fanno-line calculation a manufacturer-supplied friction factor of $f = 0.0138$ was used for the alumina tubing. The flow properties at the tube exit (T_0^{ex}, P_0^{ex}, and M_{ex}) were used as the inflow boundary conditions for the grid area from $Y/R_j = 0.0$ to 1.0, representing the exit of the alumina tube. In previous jet studies the details of the flow in the transonic region at the orifice exit have been shown to have little influence on the core flow region located more than a nozzle diameter downstream.[8] Thus, in the interest of simplicity a uniform velocity profile with no transverse velocity component (slug flow) was used. For the remainder of the grid inlet, a coflow of air at $T_{cf} = T_w = 500$ K, $P_{cf} = P_b = 11.07$ kPa, and $M_{cf} = 0.01$ was introduced. The coflow served to stabilize the calculation without altering the jet flowfield. The temperature of the coflow was arbitrarily set equal to the measured temperature of the jet chamber wall, and the pressure was set equal to the measured backpressure in the jet chamber.

Outlet

All gradients in the X direction at the outlet boundary were set equal to zero by using the values obtained from the preceding grid plane.

Line of Symmetry

All gradients in the Y direction and the transverse velocity component along the line of symmetry were set equal to zero.

Wall

No-slip boundary conditions were imposed along the grid plane representing the outer wall of the jet chamber. The temperature and pressure along the wall were set equal to those of the coflow.

Results

Calculated results for the stoichiometric case $\Phi = 1$ are presented here because this equivalence ratio gives the highest temperatures and velocities. Contours of Mach number and temperature are shown in Fig. 5. Centerline values are plotted independently to better illustrate the wide range of thermodynamic conditions that

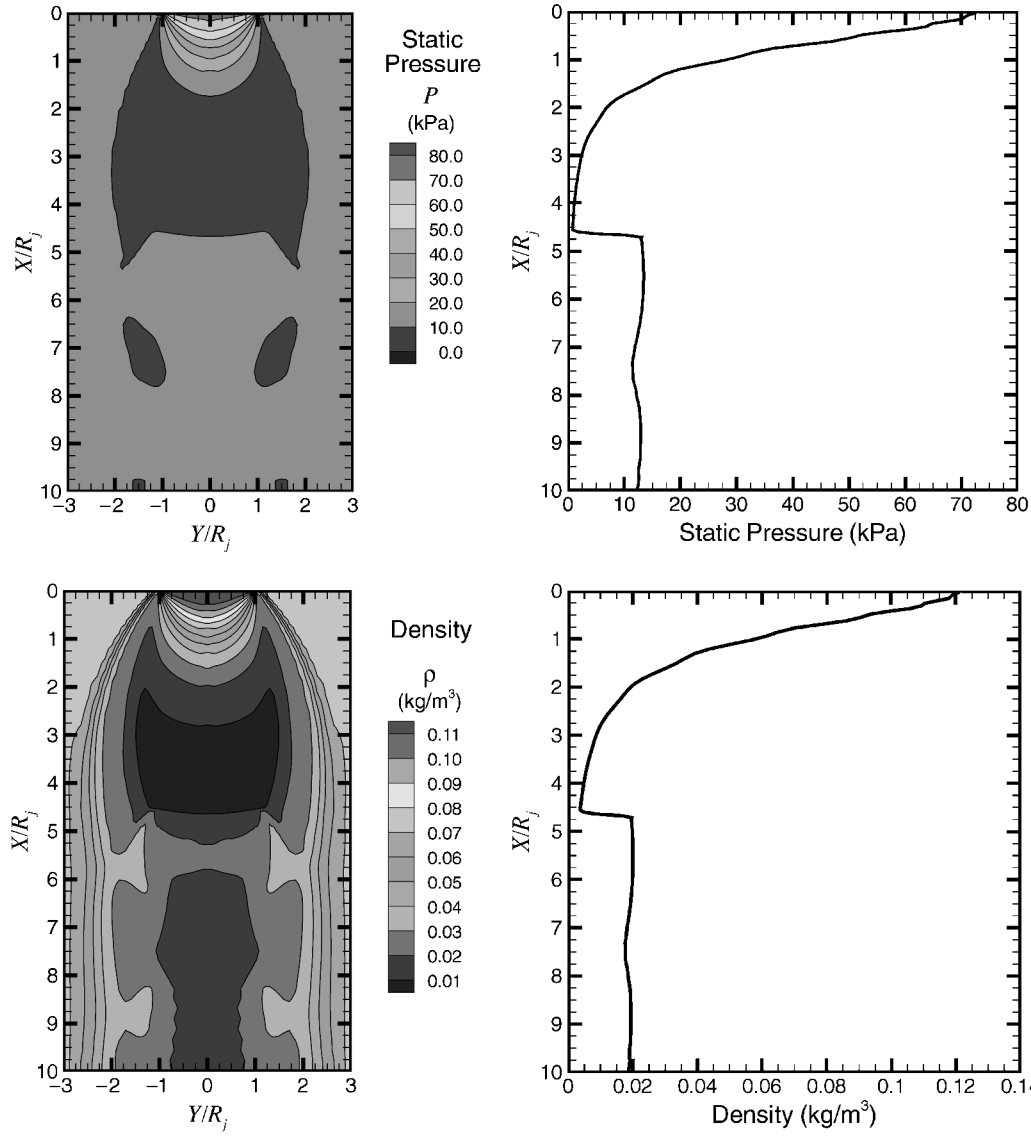

Fig. 6 Calculated contours and centerline distributions of pressure and density in the underexpanded jet, where P_0 = 160 kPa (1.58 atm), T_0 = 2000 K, P_b = 11 kPa (0.11 atm), and Φ = 1.0 (H_2/Air).

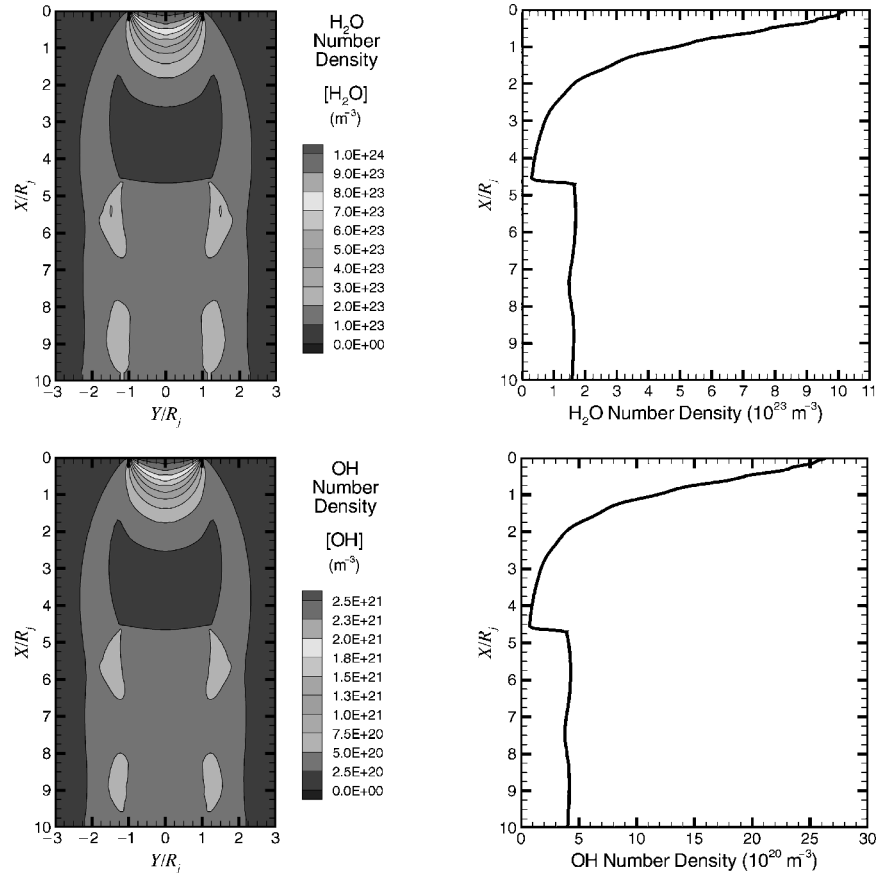

Fig. 7 Calculated contours and centerline distributions of H_2O and OH number density in the underexpanded jet, where $P_0 = 160$ kPa (1.58 atm), $T_0 = 2000$ K, $P_b = 11$ kPa (0.11 atm), and $\Phi = 1.0$ (H_2/Air).

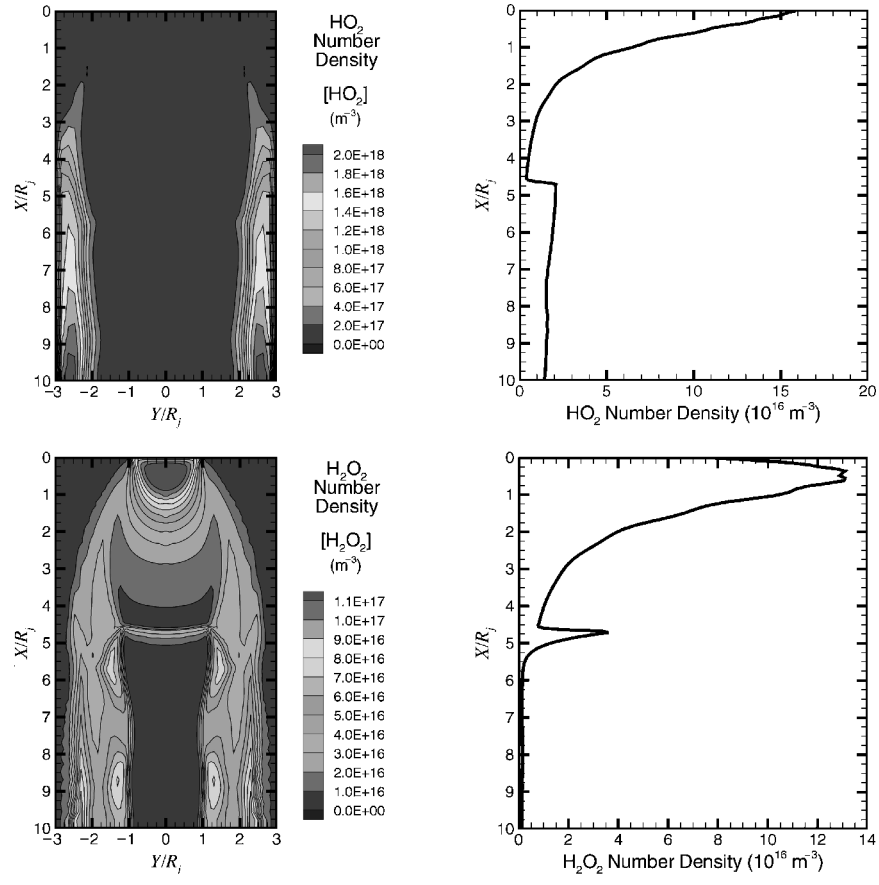

Fig. 8 Calculated contours and centerline distributions of HO_2 and H_2O_2 number density in the underexpanded jet, where $P_0 = 160$ kPa (1.58 atm), $T_0 = 2000$ K, $P_b = 11$ kPa (0.11 atm), and $\Phi = 1.0$ (H_2/Air).

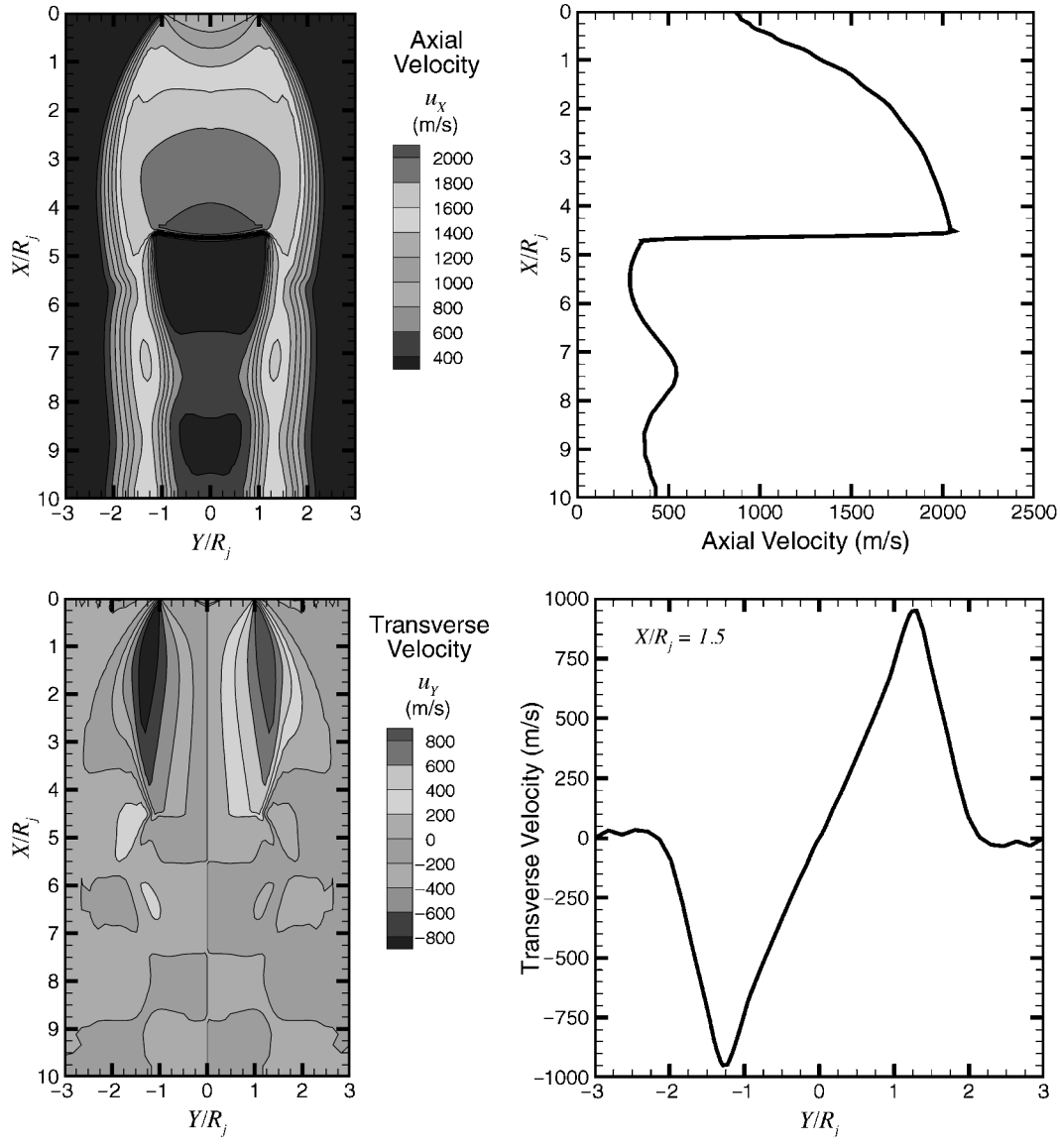

Fig. 9 Calculated contours of axial and transverse velocity, centerline distribution of axial velocity, and cross-sectional distribution of transverse velocity for $X/R_j = 1.5$ in the underexpanded jet, where $P_0 = 160$ kPa (1.58 atm), $T_0 = 2000$ K, $P_b = 11$ kPa (0.11 atm), and $\Phi = 1.0$ (H_2/Air).

is representative of supersonic flows and freejet expansions. The Mach-number ranges from $M = 1$ at the exit of the alumina tube to $M = 4$ in the core just before the Mach disk over a distance of ~4.5 jet radii, while the temperature varies from 1750 to 500 K. Contours of pressure and density are shown in Fig. 6. The pressure varies from 72.8 to 2.7 kPa, and the density varies from 0.12 to 0.004 kg/m^3 in the jet core. Contours of H_2O and OH number density are shown in Fig. 7, and contours of HO_2 and H_2O_2 number density are shown in Fig. 8. The OH number density varies by an order of magnitude from 2.5(10)^{21} m^{-3} in the high-density region at the exit of the alumina tube to 1.0(10)^{20} m^{-3} just before the Mach disk. The number densities of the other minor species, except for H_2O_2, follow the same general trend as the OH number density. The concentration of H_2O_2 decreases rapidly behind the Mach disk as a result of its relatively rapid and highly temperature-dependent rate of dissociation. Because the actual number density of H_2O_2 is relatively low, deviations in its concentration from the general trend do not appreciably affect the concentrations of the other species. Contours of the axial and transverse velocity components are shown in Fig. 9. The axial velocity varies from 880 to 2000 m/s through the jet core, and the transverse velocity peaks at 950 m/s near the barrel shock that forms the inner boundary of the jet core.

Figure 10 shows a comparison between calculated centerline OH mole fraction and axial velocity distributions for finite-rate and frozen chemistry solutions. For the finite-rate calculation the OH mole fraction along the centerline of the jet core decreases by 8% from $X/R_j = 0$ to 1.6 and remains constant from $X/R_j > 1.6$ to the Mach disk. In contrast, chemical equilibrium values of the OH mole fraction vary by 11 orders of magnitude from the high-pressure, high-temperature flow at the nozzle exit to the low-pressure, low-temperature flow just upstream of the Mach disk. Hence, the flow in the jet core is essentially chemically frozen. The comparison between the centerline axial velocity distributions for the finite-rate and frozen-flow solutions, including both the frozen SPARK solution and a method of characteristics solution using $\gamma_f = 1.25$ and $R_f = 339.3$ J/kg · K, clearly indicates that the velocity is not affected by the small amount of chemical reaction in the jet core.

Owing to the heat transfer through the combustion chamber and alumina nozzle tube, the actual source temperature used for the jet calculation is less than the stoichiometric adiabatic flame temperature (H_2/Air) of 2405 K. Because the actual heat loss was unknown, an effective source temperature T_0 was deduced by varying its value until the calculated velocity profile in the jet core matched the values measured using an OH LIF technique.[44] This procedure for deducing the effective source temperature by comparison of calculated and measured core velocity profiles is valid for the following reasons. The velocity is given by

$$u_X = M\sqrt{\gamma_f R_f T} \tag{1}$$

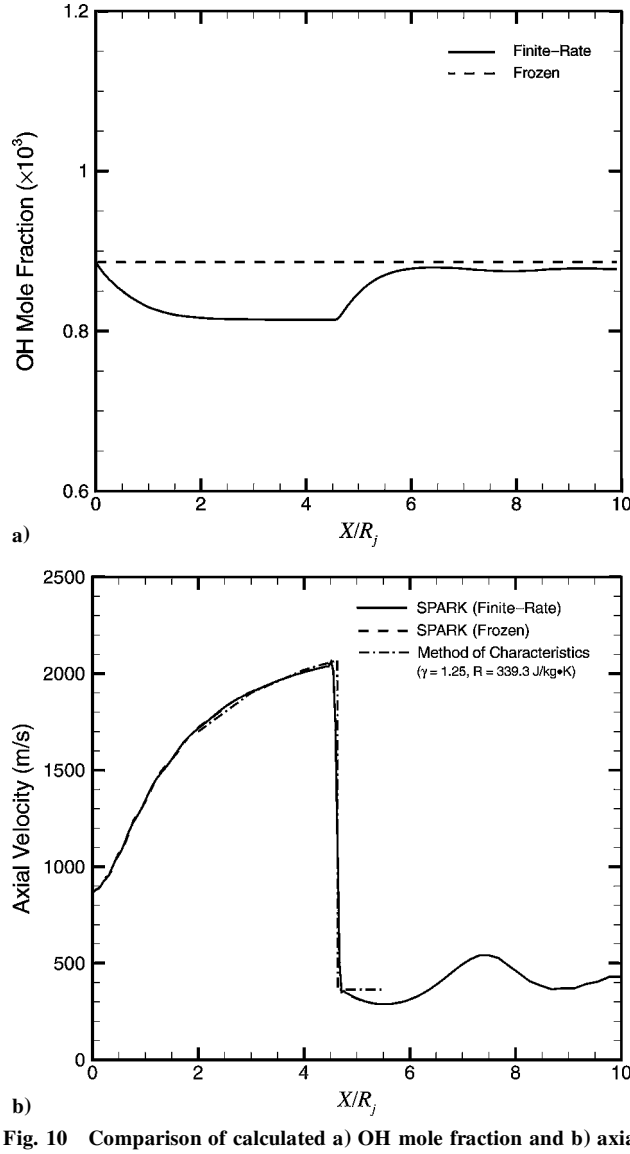

Fig. 10 Comparison of calculated a) OH mole fraction and b) axial velocity along the centerline of the underexpanded jet for finite-rate and frozen chemistry solutions.

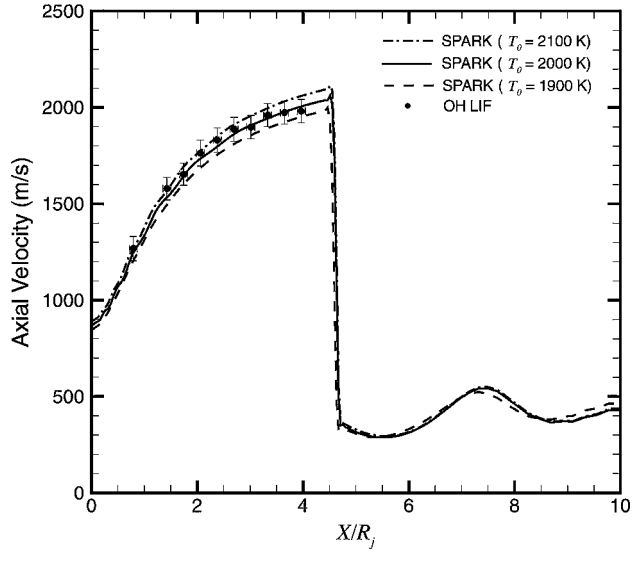

Fig. 11 Calculated axial velocity distributions for $\Phi = 1.0$, $P_0 = 160$ kPa, $P_b = 11$ kPa, and three total temperatures—$T_0 = 1900$, 2000, and 2100 K—compared with the measured axial velocity profile.

where M is the local Mach number, γ_f is the frozen specific heat ratio, R_f is the frozen gas constant, and T is the local static temperature. The centerline Mach-number distribution in the inviscid jet core is a function of γ_f alone.[8] Because the jet core has been shown to be essentially frozen and is steady, the local static temperature is determined by the local Mach number and the frozen specific heat ratio through the steady, isentropic chain.[43] The frozen specific heat ratio γ_f and the frozen (caused by frozen chemical composition) gas constant R_f are dependent only on the initial conditions in the combustion chamber T_0, P_0, and Φ. Because P_0 and Φ are measured, it is reasonable to adjust T_0 to fit the measured velocity profile in the jet core.

Figure 11 shows the measured centerline axial velocity profile in the core of the underexpanded jet, compared with calculated profiles for three values of the total temperature $T_0 = 1900$, 2000, and 2100 K. The measured experimental conditions of $P_0 = 160$ kPa, $P_b = 11$ kPa, and $\Phi = 1$ were used for all three calculations. The measured profile agrees with the calculated profile to within, on average, 1.3% for $T_0 = 2000$ K. Hence, $T_0 = 2000$ K was used for the total temperature in the combustion chamber. The calculated profiles for $T_0 = 1900$ and 2100 K indicate the sensitivity of the velocity profile to temperature. A 100-K change in total temperature produces a 56-m/s change in velocity in the jet core just before the Mach disk.

Summary

The jet facility has proven to be quite reliable except for the need for occasional repairs, with alumina cement, of cracks in the ceramic insulation lining the combustion chamber. These cracks were caused by thermal stresses, which were minimized by careful startup and shutdown procedures. However, it is recommended that the durability of the insulation and nozzle assembly be improved by having the entire assembly made from a single piece of alumina. It is also recommended to equip the jet with automatic flow meter/controllers to eliminate the tedious task of manually monitoring and adjusting the fuel and airflow rates during experiments. In addition, because the jet facility is compact, the entire setup could easily be made portable by mounting everything onto a cart equipped with a small optical bench. Only air, fuel, water, exhaust, IEEE-488, and power hookups would be necessary to make the jet available to multiple labs in a large facility.

Acknowledgments

This research was supported by NASA Grant NAG-1-795 from the Langley Research Center (LaRC), Hampton, Virginia, with G. B. Northam, technical monitor. Special thanks to J. P. Drummond for providing the SPARK code and to J. M. Donohue and G. Gauba for their assistance with the axisymmetric calculation.

References

[1]Ladenburg, R., Van Voorhis, C. C., and Winckler, J., "Interferometric Studies of Faster Than Sound Phenomena: Part II. Analysis of Supersonic Air Jets," *Physical Review*, Vol. 76, No. 5, 1949, pp. 662–677.

[2]Adamson, T. C., Jr., and Nicholls, J. A., "On the Structure of Jets from Highly Underexpanded Nozzles into Still Air," *Journal of the Aerospace Sciences*, Vol. 26, No. 1, 1959, pp. 16–24.

[3]Love, E. S., Grigsby, C. E., Lee, L. P., and Woodling, M. J., "Experimental and Theoretical Studies of Axisymmetric Free Jets," NASA TR R-6, 1959.

[4]Eastman, D. W., and Radtke, L. P., "Location of the Normal Shock Wave in the Exhaust Plume of a Jet," *AIAA Journal*, Vol. 1, No. 4, 1963, pp. 918, 919.

[5]Lewis, C. H., Jr., and Carlson, D. J., "Normal Shock Location in Underexpanded Gas and Gas-Particle Jets," *AIAA Journal*, Vol. 2, No. 4, 1964, pp. 776, 777.

[6]Bauer, A. B., "Normal Shock Location of Underexpanded Gas-Particle Jets," *AIAA Journal*, Vol. 3, No. 6, 1965, pp. 1187–1189.

[7]Crist, S., Sherman, P. M., and Glass, D. R., "Study of the Highly Underexpanded Sonic Jet," *AIAA Journal*, Vol. 4, No. 1, 1966, pp. 68–71.

[8]Ashkenas, H., and Sherman, F. S., "The Structure and Utilization of Supersonic Free Jets in Low Density Wind Tunnels," *Experimental Methods in Rarefied Gas Dynamics*, Vol. 2, Academic Press, New York, 1966, pp. 84–104.

[9]Werle, M. J., Shaffer, D. G., and Driftmyer, R. T., "Freejet Terminal Shocks," *AIAA Journal*, Vol. 8, No. 12, 1970, pp. 2295–2297.

[10]Davidor, W., and Penner, S. S., "Shock Standoff Distances and Mach-Disk Diameters in Underexpanded Sonic Jets," *AIAA Journal*, Vol. 9, No. 8, 1971, pp. 1651–1653.

[11]Abbett, M., "Mach Disk in Underexpanded Exhaust Plumes," *AIAA Journal*, Vol. 9, No. 3, 1971, pp. 512–514.

[12]Fox, J. H., "On the Structure of Jet Plumes," *AIAA Journal*, Vol. 12, No. 1, 1974, pp. 105–107.

[13]Addy, A. L., "Effects of Axisymmetric Sonic Nozzle Geometry on Mach Disk Characteristics," *AIAA Journal*, Vol. 19, No. 1, 1981, pp. 121, 122.

[14]Wlezien, R. W., and Kibens, V., "Influence of Nozzle Asymmetry on Supersonic Jets," *AIAA Journal*, Vol. 26, No. 1, 1988, pp. 27–33.

[15]Krothapalli, A., Buzyna, G., and Lourenco, L., "Streamwise Vortices in an Underexpanded Axisymmetric Jet," *Physics of Fluids A*, Vol. 3, No. 8, 1991, pp. 1848–1851.

[16]Ashratov, E. A., "Calculation of Axisymmetric Jet Leaving a Nozzle at a Jet Pressure Lower Than Pressure in Medium," *Fluid Dynamics*, Vol. 1, No. 1, 1966, pp. 113–115.

[17]Chang, I. S., and Chow, W. L., "Mach Disk from Underexpanded Axisymmetric Nozzle Flow," *AIAA Journal*, Vol. 12, No. 8, 1974, pp. 1079–1082.

[18]Dash, S. M., Wolf, D. E., and Seiner, J. M., "Analysis of Turbulent Underexpanded Jets, Part I: Parabolized Navier–Stokes Model, SCIPVIS," *AIAA Journal*, Vol. 23, No. 4, 1985, pp. 505–514.

[19]Dash, S. M., and Wolf, D. E., "Interactive Phenomena in Supersonic Jet Mixing Problems, Part I: Phenomenology and Numerical Modeling Techniques," *AIAA Journal*, Vol. 22, No. 7, 1984, pp. 905–913.

[20]Seiner, J. M., Dash, S. M., and Wolf, D. E., "Analysis of Turbulent Underexpanded Jets, Part II: Shock Noise Features Using SCIPVIS," *AIAA Journal*, Vol. 23, No. 5, 1985, pp. 669–677.

[21]Chuech, S. G., Lai, M. C., and Faeth, G. M., "Structure of Turbulent Sonic Underexpanded Free Jets," *AIAA Journal*, Vol. 27, No. 5, 1989, pp. 549–559.

[22]Hsu, A. T., and Liou, M. S., "Computational Analysis of Underexpanded Jets in the Hypersonic Regime," *Journal of Propulsion and Power*, Vol. 7, No. 2, 1991, pp. 297–299.

[23]McDaniel, J. C., Baganoff, D., and Byer, R. L., "Density Measurement in Compressible Flows Using Off-Resonance Laser-Induced Fluorescence," *Physics of Fluids*, Vol. 25, No. 7, 1982, pp. 1105–1107.

[24]McDaniel, J. C., "Quantitative Measurement of Density and Velocity in Compressible Flows Using Laser-Induced Iodine Fluorescence," AIAA Paper 83-0049, Jan. 1983.

[25]McDaniel, J. C., Hiller, B., and Hanson, R. K., "Simultaneous Multiple-Point Velocity Measurements Using Laser-Induced Iodine Fluorescence," *Optics Letters*, Vol. 8, No. 1, 1983, pp. 51–53.

[26]Hiller, B., and Hanson, R. K., "Simultaneous Planar Measurements of Velocity and Pressure Fields in Gas Flows Using Laser-Induced Fluorescence," *Applied Optics*, Vol. 27, No. 1, 1988, pp. 33–48.

[27]Fletcher, D. G., "Spatially-Resolved, Nonintrusive Measurements in a Nonreacting Scramjet Combustor Using Laser-Induced Iodine Fluorescence," Ph.D. Dissertation, Dept. of Mechanical and Aerospace Engineering, Univ. of Virginia, Charlottesville, 1989.

[28]Paul, P. H., Lee, M. P., and Hanson, R. K., "Molecular Velocity Imaging of Supersonic Flows Using Pulsed Planar Laser-Induced Fluorescence of NO," *Optics Letters*, Vol. 14, No. 9, 1989, pp. 417–419.

[29]DiRosa, M. D., Chang, A. Y., and Hanson, R. K., "CW Dye Laser Technique for Simultaneous, Spatially-Resolved Measurements of Temperature, Pressure, and Velocity of NO in an Underexpanded Free Jet," AIAA Paper 92-0006, Jan. 1992.

[30]Cheng, S., Zimmermann, M., and Miles, R. B., "Supersonic-Nitrogen Flow-Field Measurements with the Resonant Doppler Velocimeter," *Applied Physics Letters*, Vol. 43, No. 2, 1983, pp. 143–145.

[31]Miles, R. B., Connors, J., Markowitz, E., Howard, P., and Roth, G., "Instantaneous Supersonic Velocity Profiles in an Underexpanded Sonic Air Jet by Oxygen Flow Tagging," *Physics of Fluids A*, Vol. 1, No. 2, 1989, pp. 389–393.

[32]Miles, R. B., Connors, J. J., Markovitz, E. C., Howard, P. J., and Roth, G. J., "Instantaneous Profiles and Turbulence Statistics of Supersonic Free Shear Layers by Raman Excitation Plus Laser-Induced Electronic Fluorescence (RELIEF) Velocity Tagging of Oxygen," *Experiments in Fluids*, Vol. 8, 1989, pp. 17–24.

[33]Goss, L. P., Chen, T. H., Trump, D. D., and Sarka, B., "Flow-Tagging Velocimetry Using UV-Photodissociation of Water Vapor," AIAA Paper 91-0355, Jan. 1991.

[34]Moosmüller, H., Herring, G. C., and She, C. Y., "Two-Component Velocity Measurements in a Supersonic Nitrogen Jet with Spatially Resolved Inverse Raman Spectroscopy," *Optics Letters*, Vol. 9, No. 12, 1984, pp. 534–538.

[35]Herring, G. C., Fairbank, W. M., Jr., and She, C. Y., "Observation and Measurement of Molecular Flow Using Stimulated Raman Gain Spectroscopy," *IEEE Journal of Quantum Electronics*, Vol. QE-17, No. 10, 1981, pp. 1975, 1976.

[36]Gustafson, E. K., McDaniel, J. C., and Byer, R. L., "CARS Measurement of Velocity in a Supersonic Jet," *IEEE Journal of Quantum Electronics*, Vol. QE-17, No. 12, 1981, pp. 2258, 2259.

[37]Chang, A. Y., Battles, B. E., and Hanson, R. K., "Simultaneous Measurements of Velocity, Temperature, and Pressure Using Rapid CW Wavelength-Modulation Laser-Induced Fluorescence of OH," *Optics Letters*, Vol. 15, No. 12, 1990, pp. 706–708.

[38]Paul, P. H., and Hanson, R. K., "Applications of Planar Laser-Induced Fluorescence Imaging Diagnostics to Reacting Flows," AIAA Paper 90-1848, July 1990.

[39]Mataga, T. G., and Cattolica, R. J., "OH Rotational Temperature Measurements in a Combustion Driven Supersonic Free Jet," *Proceedings of the 13th International Colloquium on Dynamics of Explosions and Reactive Systems*, Nagoya, Japan, July–Aug. 1991.

[40]Wu, C. K., and Law, C. K., "On the Determination of Laminar Flame Speeds from Stretched Flames," *Proceedings of the 20th International Symposium on Combustion*, Combustion Inst., Pittsburgh, PA, 1984, pp. 1941–1949.

[41]Drummond, J. P., "A Two-Dimensional Numerical Simulation of a Supersonic, Chemically Reacting Mixing Layer," NASA TM 4055, 1988.

[42]Reynolds, W. C., "The Element Potential Method for Chemical Equilibrium Analysis: Implementation in the Interactive Program STANJAN—Version 3," Dept. of Mechanical Engineering, Stanford Univ., CA, 1986.

[43]Shapiro, A. H., *The Dynamics and Thermodynamics of Compressible Fluid Flow*, Vol. I, Ronald, New York, 1953.

[44]Klavuhn, K. G., Gauba, G., and McDaniel, J. C., "OH Laser-Induced Fluorescence Velocimetry Technique for Steady, High-Speed, Reacting Flows," *Journal of Propulsion and Power*, Vol. 10, No. 6, 1994, pp. 787–797.